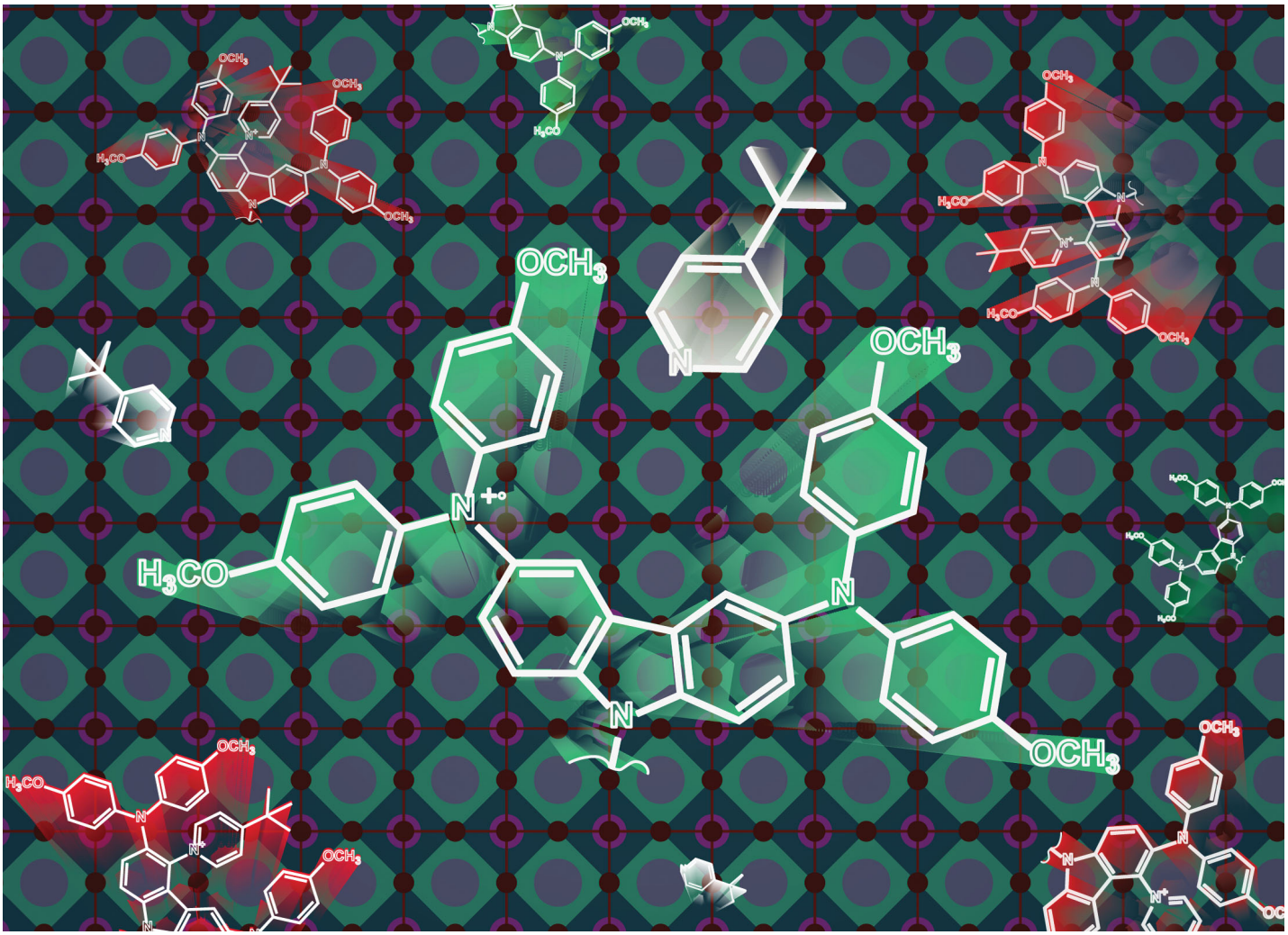

Showcasing research from the Department of Organic Chemistry, Kaunas University of Technology, Lithuania and the Group for Molecular Engineering of Functional Materials, Institute of Chemical Sciences and Engineering, École polytechnique fédérale de Lausanne, Switzerland

Pyridination of hole transporting material in perovskite solar cells questions the long-term stability

Hole transporting materials (HTMs), used in perovskite solar cells, are routinely doped with several additives. This work shows the reaction of HTM with a *tert*-butylpyridine additive, which has a negative impact on device performance.

As featured in:

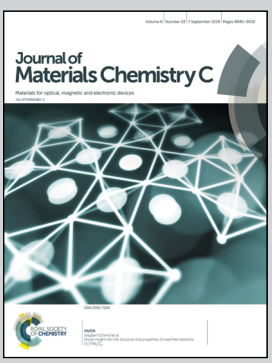

See Artiom Magomedov, Mohammad Khaja Nazeeruddin, Vytautas Getautis *et al.*, *J. Mater. Chem. C*, 2018, **6**, 8874.

ROYAL SOCIETY OF CHEMISTRY

rsc.li/materials-c

Journal of
Materials Chemistry C

COMMUNICATION

View Article Online
View Journal | View Issue

Cite this: J. Mater. Chem. C, 2018, 6, 8874

Received 9th May 2018,
Accepted 10th July 2018

DOI: 10.1039/c8tc02242a

rsc.li/materials-c

Pyridination of hole transporting material in perovskite solar cells questions the long-term stability†

Artiom Magomedov,*[a] Ernestas Kasparavičius,[a] Kasparas Rakstys,[b] Sanghyun Paek,[b] Natalia Gasilova,[b] Kristijonas Genevičius,[c] Gytis Juška,[c] Tadas Malinauskas,[a] Mohammad Khaja Nazeeruddin *[b] and Vytautas Getautis *[a]

In this work, for the first time, reactive radical-cation species present in hole-transporting materials were shown to react with *tert*-butylpyridine additive, routinely used in hole transporting layer composition. As a result, new pyridinated products were isolated and characterized by NMR and MS analysis. Additionally, their optical and photophysical properties (*i.e.*, solid-state ionization potentials (I_p), cyclic voltammetry (CV), UV/vis characteristics, and conductivities) were determined. Formation of the pyridinated products was confirmed in the aged perovskite solar cells by means of mass spectrometry, and shown to have negative influence on the overall device performance. We believe that these findings will help improve the stability of perovskite devices by either molecular engineering of hole-transporting materials or utilization of less-reactive or sterically hindered pyridine derivatives.

Perovskite solar cells (PSCs) are efficient, yet achieving high stability is still challenging.[1] The efficiencies of PSCs over the past decade have reached an impressive 22.7%[2] for small devices, 19.6%[2] for 1 cm^2 devices and 12.1%[3] for >36 cm^2 mini-modules. Various scalable techniques (*e.g.*, blade-coating[4] and roll-to-roll[5] techniques) that have been applied for the deposition of perovskites promise suitable market applications. Further improvements in the stability of the devices are crucial for the successful commercialization of PSCs.

Although moisture and oxygen penetration can be efficiently suppressed by encapsulation,[6–8] the stability of the materials and interfaces is essential. Significantly improved stability of the perovskite compositions have been achieved using multi-cation (methylammonium, formamidinium, cesium,[9] and rubidium[10]). With this increase of the perovskite stability, the hole-selective contact is typically considered as the main reason for efficiency loss, which is supported by the excellent long-term stability of hole-transporting material-free devices; however, at the cost of significantly reduced efficiency of the PSCs.[11,12]

The exact reasons for the degradation of the hole-selective contact are still unclear. Recently, K. Domanski *et al.* demonstrated that hole transporting material (HTM) becomes permeable to the gold migration at high temperatures.[13] However, gold-free architectures with carbon-based back electrode, which avoid fast degradation, still steadily degrade.[14,15] Thus, attention must be paid to the increase in stability of the HTM itself.

Molecules containing methoxydiphenylamine-substituted fluorene[16,17] and carbazole[18] derivatives are among the best performing HTMs, with 2,2′,7,7′-tetrakis-(*N*,*N*-di-*p*-methoxyphenylamine)-9,9′-spirobifluorene (spiro-OMeTAD) remaining the most popular HTM. Other examples includes azomethine derivative EDOT-OMeTPA,[19] fluorene-dithiophene-based FDT,[16] and chemically more stable phthalocyanine-based HTMs.[20–22] Recently, our group synthesized the promising HTM **V886**,[23] which is a cheaper alternative to spiro-OMeTAD. However, above mentioned HTMs in their pristine form show low performance due to the low conductivity. To overcome this disadvantage, dopants, such as lithium bis(trifluoromethane)sulfonamide[24] (LiTFSI), FK209[25] and *tert*-butylpyridine (tBP), are typically added before layer formation. While LiTFSI and FK209 act as oxidizing agents,[26] improving the HTM conductivity; the role of tBP is still under investigation. Despite the positive effects on the overall performance of solar cells, dopants typically result in reduced long-term performance compared with dopant-free HTM based devices.[27–29]

Even though tBP has been used in PSCs to improve overall device performance, the exact role of tBP remains unclear, and several different mechanisms have been proposed. Since the first application in a dye-sensitized solar cell (DSSC)[30] and further transition to a solid-state DSSC,[24] tBP has been used without understanding this underlying mechanism. In 2014,

[a] Department of Organic Chemistry, Kaunas University of Technology, Radvilenu pl. 19, Kaunas 50254, Lithuania. E-mail: artiom.magomedov@ktu.lt, vytautas.getautis@ktu.lt
[b] Group for Molecular Engineering of Functional Materials, Institute of Chemical Sciences and Engineering, École Polytechnique Fédérale de Lausanne, CH-1951 Sion, Switzerland. E-mail: mdkhaja.nazzeruddin@epfl.ch
[c] Department of Solid State Electronics, Vilnius University, Sauletekio 9 III k, 10222 Vilnius, Lithuania

† Electronic supplementary information (ESI) available. See DOI: 10.1039/c8tc02242a

N. Noel *et al.*[31] suggested that pyridine base acts as a trap-passivation material, thus reducing recombination at the HTM/perovskite interface. In 2016, S. Wang *et al.*[32] suggested that tBP acts as a co-solvent, improving the uniformity of the spin-coated layers. Later in the same year, the positive effect of tBP was proposed[33] to result from a direct chemical interaction between tBP and the perovskite material. However, at approximately the same time,[34] corrosion of the perovskite by pyridine additives was demonstrated. All these mechanisms were supported by experimental evidence and may be complementary to one another. For the sake of further developments in the field, a more detailed and complete mechanism is still greatly demanded.

To date, no attention has been paid to the possible interaction between the HTM and tBP. Pyridine can act as a nucleophile on the heteroaromatic radical cation species formed during doping process.[35] Since both the radical cation and pyridine derivative are present in the HTM layer, the oxidized HTM and tBP can potentially chemically interact with each other, which would raise questions on the impact of tBP on the long-term stability of the HTM material and devices themselves.

In this work, for the first time, we uncover the chemical reaction between the oxidized HTM **V886** and tBP. New pyridinated compounds were formed in high yields and were isolated by standard chromatographic procedures for further characterization.

Initially, chemical interaction between tBP and model HTM compound **V990** was studied. Dimethoxydiphenylamine-substituted carbazole fragments are present in several efficient twin HTMs,[18,23] but materials with only one fragment have equivalent chemical properties and are simpler to analyse. **V990** was prepared by a simple two-step synthesis in high yield (Scheme S1, ESI†). The cation-radical form (**V990$^+$(TFSI$^-$)**) was obtained *via* oxidation with AgTFSI, adapting the procedure published by W. H. Nguyen *et al.*[36]

Next, we studied the chemical interaction between **V990$^+$(TFSI$^-$)** and tBP. To reduce the number of possible by-products and increase the speed of the reaction, **V990$^+$(TFSI$^-$)** was dissolved in pure tBP and heated at 60 °C. After 10 min color of the solution changed from intensive green to dark orange. After 20 min, the reaction was stopped, excess tBP was evaporated under reduced pressure and two products were isolated after chromatographic purification.

The structures of the formed products were analyzed by ^{1}H NMR and ^{13}C NMR spectroscopy. One product was determined to be unoxidized **V990**. In the ^{1}H NMR spectrum of the other product, down-field signals (8.98 (d, J = 6.5 Hz, 2H) and 7.86 (d, J = 6.9 Hz, 2H)), which are assigned to the pyridinium fragment, were observed. The singlet at 1.19 ppm (9H) confirmed the presence of the *tert*-butyl group in the product, suggesting a structure with one pyridinium fragment attached to **V990(tBP$^+$)(TFSI$^-$)** (Scheme 1). The full spectrum is shown in Fig. S5 in the ESI.†

T. Morofuji *et al.* proposed that the pyridination site is consistent with the lowest unoccupied molecular orbital (LUMO) of the radical cation, which was determined by density functional theory (DFT) calculations.[37] As seen in Fig. 1, the pyridination site is most likely located at the 4 position of the carbazole moiety. This conclution is supported by the ^{1}H NMR spectra. In the range of 7.96–6.16 ppm, five signals with 1H integral can be observed with the spin–spin coupling pattern (four doublets, one double doublet) well consistent with the substitution by pyridinium fragment at the 4 position of carbazole. To further confirm proposed structure, ^{13}C NMR spectra was predicted by means of DFT calculations (more details are available in the ESI†). Predicted spectra (Fig. S8, ESI†) is in good agreement with the measured NMR spectra. Characteristic signal of the carbon at the 4 position of *t*-butylpyridine ring was calculated to be at 174.34 ppm, and is in a good agreement with the experimentally measured values (172.46 ppm from dmso-d_6, and 174.36 ppm from acetone-d_6).

Based on the obtained products and reaction conditions, a reaction mechanism was proposed (Scheme 2).

The proposed mechanism predicts formation of the unoxidized **V990** and pyridinated **V990(tBP$^+$)(TFSI$^-$)** in a 1 : 1 molar ratio. Indeed, the two products were isolated in a similar ratios (38.5% and 33% yields based on the starting material).

To determine whether the same process occurs in a well-performing HTM, **V886**[23] was tested under identical

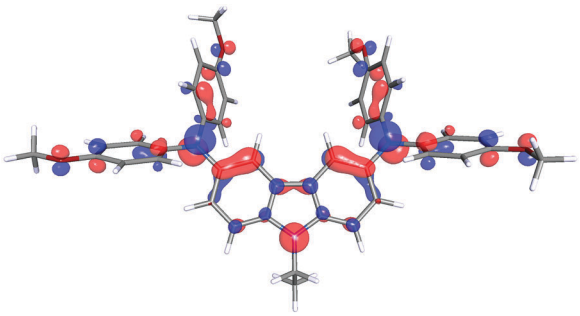

Fig. 1 The lowest unoccupied molecular orbitals of **V990$^+$** obtained by DFT calculations (B3LYP/def2-SVP). Isovalue = 0.04.

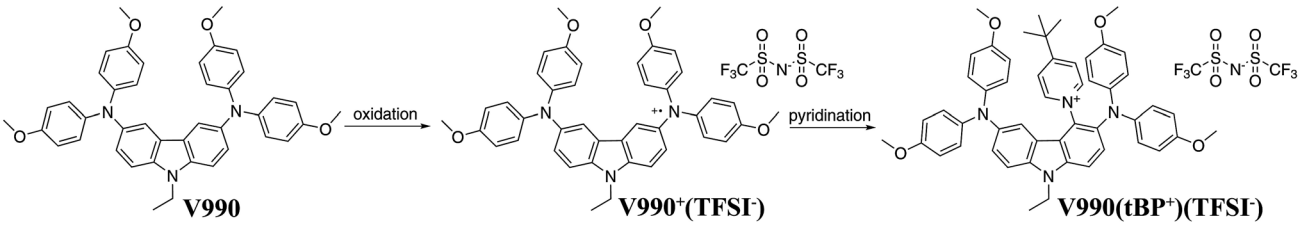

Scheme 1 Oxidation and C–H pyridination of the dimethoxydiphenylamine-substituted carbazole fragment in **V990**.

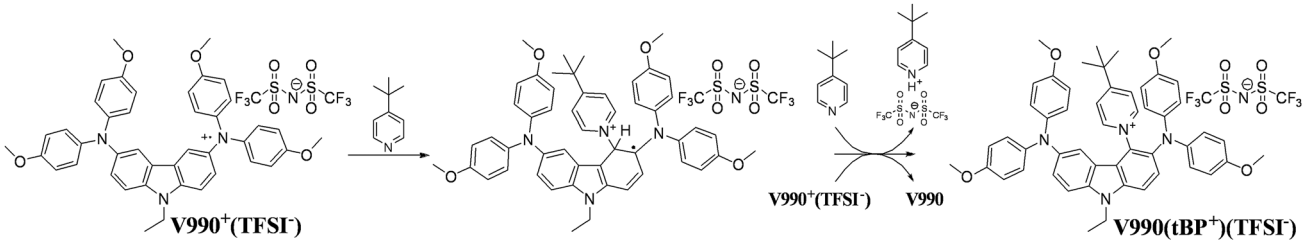

Scheme 2 Proposed mechanism of the C–H pyridination reaction.

reaction conditions. C–H pyridination of **V886**$^{2+}$(**TFSI**$^-$)$_2$ occurred in the same manner, two pyridinated products were isolated and characterized by NMR. The mono- (**V886(tBP**$^+$**)(TFSI**$^-$**)**) and dipyridinated (**V886(tBP**$^+$**)**$_2$**(TFSI**$^-$**)**$_2$) derivatives were obtained in 37.9% and 17.1% yields, respectively (Fig. 2). Additionally, as in the previous case, unoxidized **V886** was isolated in a 20.5% yield. More details, as well as UV/vis and NMR spectra, are available in the ESI.†

Additionally, we studied the effect of this process on the electrical properties of the HTM. Presence of the oxidized species increase the conductivity of the HTM,[23] resulting in better PSC performance. The conductivities of the formed pyridinated products **V886(tBP**$^+$**)(TFSI**$^-$**)** and **V886(tBP**$^+$**)**$_2$**(TFSI**$^-$**)**$_2$ were on the order of 10^{-9} S cm^{-1} (Table S2, ESI†), which is significantly lower than the conductivity of oxidized **V886** (4.2×10^{-5} S cm^{-1}).[23]

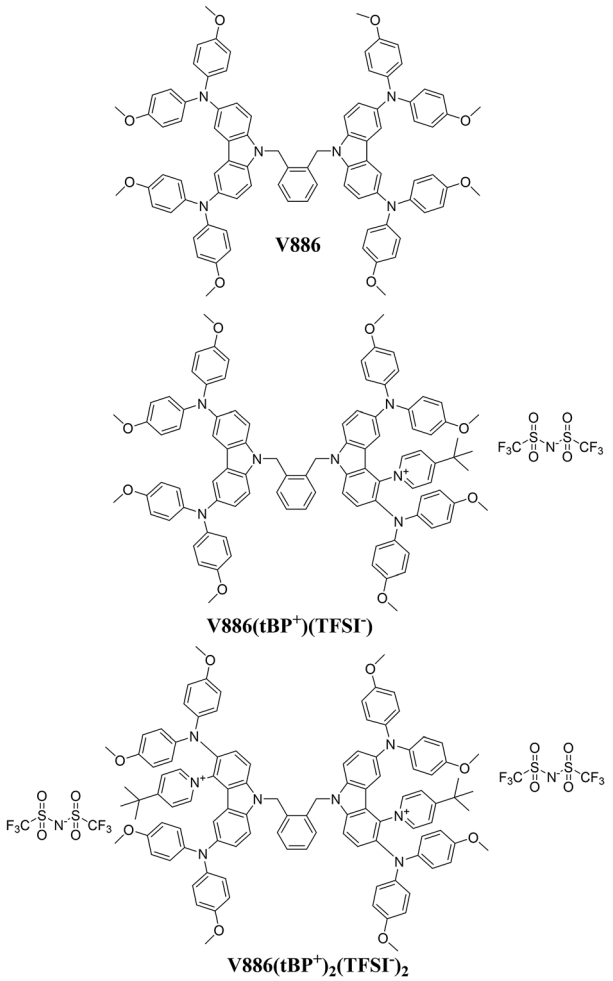

Fig. 2 Structures of the **V886**, **V886(tBP**$^+$**)(TFSI**$^-$**)**, and **V886(tBP**$^+$**)**$_2$**(TFSI**$^-$**)**$_2$.

To estimate the energy levels of these materials, their oxidation potentials were measured in solution using cyclic voltammetry (CV) (Fig. S18 and Table S1, ESI†). **V886** showed two quasi-reversible oxidation signals at 0.085 and 0.272 V *vs.* Fc/Fc$^+$ (Fc = ferrocene). For **V886(tBP**$^+$**)(TFSI**$^-$**)**, three redox waves were observed: the first two signals were very close in value to those of **V886**, and the third oxidation process occurred at 0.527 V *vs.* Fc/Fc$^+$. **V886(tBP**$^+$**)**$_2$**(TFSI**$^-$**)**$_2$ showed only two waves at 0.292 and 0.599 V *vs.* Fc/Fc$^+$. These results agree with the structures of the materials, where two similar fragments are interconnected by a bridging unit. CV data in combination with the optical spectroscopy data was used to determine HOMO/LUMO levels of the molecules and the results are presented in Table S1 (ESI†). It can be seen, that pyridination of the **V886** results in more negative HOMO level (−5.32, −5.34, and −5.53 eV for **V886**, **V886(tBP**$^+$**)(TFSI**$^-$**)**, and **V886(tBP**$^+$**)**$_2$**(TFSI**$^-$**)**$_2$ respectively). In addition, bandgap of the **V886** (2.72 eV) becomes narrower for both **V886(tBP**$^+$**)(TFSI**$^-$**)** (1.70 eV) and **V886(tBP**$^+$**)**$_2$**(TFSI**$^-$**)**$_2$ (1.78 eV). As a consequence lower LUMO levels were observed for **V886(tBP**$^+$**)(TFSI**$^-$**)**, and **V886(tBP**$^+$**)**$_2$**(TFSI**$^-$**)**$_2$ (−3.64, and −3.75 eV respectively) compared with **V886** (−2.60 eV). Such change in LUMO energy level could lead to reduced electron-blocking properties of the HTM.

For better representation of the material energetics, the solid-state ionization potential (I_p) values were measured by photoelectron spectroscopy in air (PESA). For **V886(tBP**$^+$**)(TFSI**$^-$**)**, the I_p value was 5.4 eV, and for **V886(tBP**$^+$**)**$_2$**(TFSI**$^-$**)**$_2$, the I_p value was close to the measurement limit of our equipment, estimated to be ∼5.7 eV (Fig. S17, ESI†), which is higher than that of the **V886** (5.04 eV[23]). High I_p value is unfavorable for the charge extraction from the perovskite absorber material, due to the mismatch with the perovskite valence band edge energy. Therefore it can be expected that pyridinated species would serve as a trap-states for the charges, reducing overall PSC performance.

To check, if pyridinated products can be formed in the device, PSCs with **V886** as a HTM were prepared, following the recently published procedure.[34] Initially, device showed 17.5% PCE, which after thermal stress (80 °C in air for 340 h) dropped down to 13.81% PCE (Fig. S20, ESI†). The aged PSC was washed with the small amount of THF, followed by filtration of the resulting

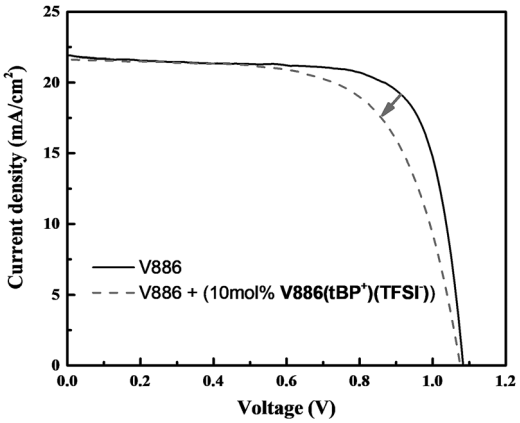

Fig. 3 *J–V* characteristics of PSC with **V886**, and **V886** + (10 mol% **V886(tBP$^+$)(TFSI$^-$)**) as a HTL.

extract. Concentrated sample was then directly subjected to the MS analysis. As can be seen from the Fig. S22 (ESI†), weak signal at 1478.856 *m*/*z* can be observed, which is attributed to the **V886(tBP$^+$)** cation (1478.6694 Da). To further confirm nature of this signal, high resolution MS/MS analysis was performed (Fig. S23, ESI†) and the fragmentation pattern confirmed that the observed signal arises from the **V886(tBP$^+$)(TFSI$^-$)**, the dipyridinated product **V886(tBP$^+$)$_2$(TFSI$^-$)$_2$** was not found by MS.

To exclude other degradation pathways, and to reveal the influence of the pyridination on the overall performance of the PSC, we have prepared a fresh devices with **V886** HTM, where 10 mol% of **V886(tBP$^+$)(TFSI$^-$)** was added to the hole transporting layer (HTL) composition before film formation, mimicking the aging process. Reference cell with **V886** showed 17.5% PCE (V_{oc} 1.083 V; J_{sc} 21.91 mA cm^{-1}; FF 73.7%), while device with 10 mol% of the **V886(tBP$^+$)(TFSI$^-$)** additive showed reduced performance of 15.23% PCE (V_{oc} 1.075 V;J_{sc} 21.64 mA cm^{-1}; FF 65.4%) (Fig. 3). We note that such a drop in performance could be attributed to the presence of less conductive **V886(tBP$^+$)(TFSI$^-$)** species in the HTM film, additionally, higher I_p of **V886(tBP$^+$)(TFSI$^-$)** also has detrimental effect on charge injection efficiency to the HTM from the perovskite layer.

Additionally, the pyridination process was observed for the oxidized spiro-OMeTAD and some other oxidized HTM representatives. More detailed empirical study was published separately.[38]

In conclusion, for the first time we show that oxidized HTM species are prone to chemically interact with tBP additive, forming new pyridinated products. In addition, it was shown that the same process *in situ* occurs in the PSCs at elevated temperatures during the relatively short aging time, and that the formation of the pyridinated product **V886(tBP$^+$)(TFSI$^-$)** has a negative impact on the device performance. These findings raise new questions about the long-term stability of PSCs, particularly the stability of organic HTMs upon doping. To avoid negative impacts, we suggest using less-nucleophilic or sterically hindered pyridine derivatives[34] or substitute the active hydrogen sites of the HTM.

Conflicts of interest

There are no conflicts to declare.

Acknowledgements

The authors acknowledge funding from the Research Council of Lithuania *via* Grant (No. LAT-07/2016). We thank E. Kamarauskas for his help with ionization potential measurements.

Notes and references

1 Y. Yang and J. You, *Nature*, 2017, **544**, 155–156.
2 NREL efficiency chart, https://www.nrel.gov/pv/assets/images/efficiency-chart.png, (accessed 6 February 2018).
3 SJTU Team, http://en.sjtu.edu.cn/news/a-breakthrough-in-large-area-perovskite-solar-panels-by-sjtu-team/, (accessed 2 March 2018).
4 M. Yang, Z. Li, M. O. Reese, O. G. Reid, D. H. Kim, S. Siol, T. R. Klein, Y. Yan, J. J. Berry, M. F. A. M. van Hest and K. Zhu, *Nat. Energy*, 2017, **2**, 17038.
5 Solliance, http://solliance.eu/solliance-sets-world-record-for-roll-to-roll-produced-perovskite-based-solar-cells-with-a-stabilized-efficiency-of-126/, (accessed 2 March 2018).
6 I. Hwang, I. Jeong, J. Lee, M. J. Ko and K. Yong, *ACS Appl. Mater. Interfaces*, 2015, **7**, 17330–17336.
7 H. C. Weerasinghe, Y. Dkhissi, A. D. Scully, R. A. Caruso and Y.-B. Cheng, *Nano Energy*, 2015, **18**, 118–125.
8 F. Bella, G. Griffini, J.-P. Correa-Baena, G. Saracco, M. Gratzel, A. Hagfeldt, S. Turri and C. Gerbaldi, *Science*, 2016, **354**, 203–206.
9 M. Saliba, T. Matsui, J.-Y. Seo, K. Domanski, J.-P. Correa-Baena, M. K. Nazeeruddin, S. M. Zakeeruddin, W. Tress, A. Abate, A. Hagfeldt and M. Grätzel, *Energy Environ. Sci.*, 2016, **9**, 1989–1997.
10 M. Saliba, M. Saliba, T. Matsui, K. Domanski, J.-Y. Seo and A. Ummadisingu, *Science*, 2016, **354**, 206–209.
11 X. Li, M. Tschumi, H. Han, S. S. Babkair, R. A. Alzubaydi, A. A. Ansari, S. S. Habib, M. K. Nazeeruddin, S. M. Zakeeruddin and M. Grätzel, *Energy Technol.*, 2015, **3**, 551–555.
12 S. G. Hashmi, A. Tiihonen, D. Martineau, M. Ozkan, P. Vivo, K. Kaunisto, V. Ulla, S. M. Zakeeruddin, M. Grätzel, P. D. Lund, M. Grätzel, M. Duan, J. Zhao, X. Li and H. Han, *J. Mater. Chem. A*, 2017, **5**, 4797–4802.
13 K. Domanski, J.-P. Correa-Baena, N. Mine, M. K. Nazeeruddin, A. Abate, M. Saliba, W. Tress, A. Hagfeldt and M. Grätzel, *ACS Nano*, 2016, **10**, 6306–6314.
14 K. Aitola, K. Domanski, J. P. Correa-Baena, K. Sveinbjörnsson, M. Saliba, A. Abate, M. Grätzel, E. Kauppinen, E. M. J. Johansson, W. Tress, A. Hagfeldt and G. Boschloo, *Adv. Mater.*, 2017, **29**, 1606398.
15 S. Gholipour, J.-P. Correa-Baena, K. Domanski, T. Matsui, L. Steier, F. Giordano, F. Tajabadi, W. Tress, M. Saliba, A. Abate, A. Morteza Ali, N. Taghavinia, M. Grätzel and A. Hagfeldt, *Adv. Energy Mater.*, 2016, **6**, 1601116.

16 M. Saliba, S. Orlandi, T. Matsui, S. Aghazada, M. Cavazzini, J.-P. Correa-Baena, P. Gao, R. Scopelliti, E. Mosconi, K.-H. Dahmen, F. De Angelis, A. Abate, A. Hagfeldt, G. Pozzi, M. Graetzel and M. K. Nazeeruddin, *Nat. Energy*, 2016, **1**, 15017.
17 T. Malinauskas, M. Saliba, T. Matsui, M. Daskeviciene, S. Urnikaite, P. Gratia, R. Send, H. Wonneberger, I. Bruder, M. Graetzel, V. Getautis and M. K. Nazeeruddin, *Energy Environ. Sci.*, 2016, **9**, 1681–1686.
18 B. Xu, E. Sheibani, P. Liu, J. Zhang, H. Tian, N. Vlachopoulos, G. Boschloo, L. Kloo, A. Hagfeldt and L. Sun, *Adv. Mater.*, 2014, **26**, 6629–6634.
19 M. L. Petrus, T. Bein, T. J. Dingemans, P. Docampo, M. M. Wienk, R. A. J. Janssen, Y. Olivier, T. J. Savenije, L. D. A. Siebbeles, N. C. Greenham and T. J. Dingemans, *J. Mater. Chem. A*, 2015, **3**, 12159–12162.
20 E. Nouri, Y.-L. Wang, Q. Chen, J.-J. Xu, G. Paterakis, V. Dracopoulos, Z.-X. Xu, D. Tasis, M. R. Mohammadi and P. Lianos, *Electrochim. Acta*, 2017, **233**, 36–43.
21 E. Nouri, J. V. S. Krishna, C. V. Kumar, V. Dracopoulos, L. Giribabu, M. R. Mohammadi and P. Lianos, *Electrochim. Acta*, 2016, **222**, 875–880.
22 K. T. Cho, O. Trukhina, C. Roldán-Carmona, M. Ince, P. Gratia, G. Grancini, P. Gao, T. Marszalek, W. Pisula, P. Y. Reddy, T. Torres and M. K. Nazeeruddin, *Adv. Energy Mater.*, 2017, **7**, 1601733.
23 P. Gratia, A. Magomedov, T. Malinauskas, M. Daskeviciene, A. Abate, S. Ahmad, M. Grätzel, V. Getautis and M. K. Nazeeruddin, *Angew. Chem., Int. Ed.*, 2015, **54**, 11409–11413.
24 M. Grätzel, U. Bach, D. Lupo, P. Comte, J. E. Moser, F. Weissörtel, J. Salbeck and H. Spreitzer, *Nature*, 1998, **395**, 583–585.
25 J. H. Noh, N. J. Jeon, Y. C. Choi, M. K. Nazeeruddin, M. Grätzel and S. Il Seok, *J. Mater. Chem. A*, 2013, **1**, 11842.
26 A. Abate, T. Leijtens, S. Pathak, J. Teuscher, R. Avolio, M. E. Errico, J. Kirkpatrik, J. M. Ball, P. Docampo, I. McPherson and H. J. Snaith, *Phys. Chem. Chem. Phys.*, 2013, **15**, 2572.
27 K. Rakstys, S. Paek, P. Gao, P. Gratia, T. Marszalek, G. Grancini, K. T. Cho, K. Genevicius, V. Jankauskas, W. Pisula and M. K. Nazeeruddin, *J. Mater. Chem. A*, 2017, **5**, 7811–7815.
28 T. Matsui, I. Petrikyte, T. Malinauskas, K. Domanski, M. Daskeviciene, M. Steponaitis, P. Gratia, W. Tress, J.-P. Correa-Baena, A. Abate, A. Hagfeldt, M. Grätzel, M. K. Nazeeruddin, V. Getautis and M. Saliba, *ChemSusChem*, 2016, **9**, 2567–2571.
29 G.-W. Kim, G. Kang, J. Kim, G.-Y. Lee, H. Il Kim, L. Pyeon, J. Lee and T. Park, *Energy Environ. Sci.*, 2016, **9**, 2326–2333.
30 M. K. Nazeeruddin, A. Kay, I. Rodicio, R. Humphry-Baker, E. Mueller, P. Liska, N. Vlachopoulos and M. Graetzel, *J. Am. Chem. Soc.*, 1993, **115**, 6382–6390.
31 N. K. Noel, A. Abate, S. D. Stranks, E. S. Parrott, V. M. Burlakov, A. Goriely and H. J. Snaith, *ACS Nano*, 2014, **8**, 9815–9821.
32 S. Wang, M. Sina, P. Parikh, T. Uekert, B. Shahbazian, A. Devaraj and Y. S. Meng, *Nano Lett.*, 2016, **16**, 5594–5600.
33 S. N. Habisreutinger, N. K. Noel, H. J. Snaith and R. J. Nicholas, *Adv. Energy Mater.*, 2017, **7**, 1601079.
34 Y. Yue, N. Salim, Y. Wu, X. Yang, A. Islam, W. Chen, J. Liu, E. Bi, F. Xie, M. Cai and L. Han, *Adv. Mater.*, 2016, **28**, 10738–10743.
35 H. Lund, *Acta Chem. Scand.*, 1957, **11**, 1323–1330.
36 W. H. Nguyen, C. D. Bailie, E. L. Unger and M. D. McGehee, *J. Am. Chem. Soc.*, 2014, **136**, 10996–11001.
37 T. Morofuji, A. Shimizu and J. Yoshida, *J. Am. Chem. Soc.*, 2013, **135**, 5000–5003.
38 E. Kasparavicius, A. Magomedov, T. Malinauskas and V. Getautis, *Chem. – Eur. J.*, 2018, **24**, 9910–9918.

